JOURNAL OF MAGNETIC RESONANCE **131,** 272–285 (1998)
ARTICLE NO. MN981379

# Activation of Visuomotor Systems during Visually Guided Movements: A Functional MRI Study

Jutta M. Ellermann,*,§ Joel D. Siegal,‡ John P. Strupp,* Timothy J. Ebner,†,‡ and Kâmil Ugurbil*,§

*Center for Magnetic Resonance Research, †Department of Physiology, ‡Department of Neurosurgery, and §Department of Radiology, University of Minnesota, School of Medicine, Minneapolis, Minnesota 55455*

Received October 20, 1997

**The dorsal stream is a dominant visuomotor pathway that connects the striate and extrastriate cortices to posterior parietal areas. In turn, the posterior parietal areas send projections to the frontal primary motor and premotor areas. This cortical pathway is hypothesized to be involved in the transformation of a visual input into the appropriate motor output. In this study we used functional magnetic resonance imaging (fMRI) of the entire brain to determine the patterns of activation that occurred while subjects performed a visually guided motor task. In nine human subjects, fMRI data were acquired on a 4-T whole-body MR system equipped with a head gradient coil and a birdcage RF coil using a $T_2^*$-weighted EPI sequence. Functional activation was determined for three different tasks: (1) a visuomotor task consisting of moving a cursor on a screen with a joystick in relation to various targets, (2) a hand movement task consisting of moving the joystick without visual input, and (3) a eye movement task consisting of moving the eyes alone without visual input. Blood oxygenation level-dependent (BOLD) contrast-based activation maps of each subject were generated using period cross-correlation statistics. Subsequently, each subject's brain was normalized to Talairach coordinates, and the individual maps were compared on a pixel by pixel basis. Significantly activated pixels common to at least four out of six subjects were retained to construct the final functional image. The pattern of activation during visually guided movements was consistent with the flow of information from striate and extrastriate visual areas, to the posterior parietal complex, and then to frontal motor areas. The extensive activation of this network and the reproducibility among subjects is consistent with a role for the dorsal stream in transforming visual information into motor behavior. Also extensively activated were the medial and lateral cerebellar structures, implicating the cortico–ponto–cerebellar pathway in visually guided movements. Thalamic activation, particularly of the pulvinar, suggests that this nucleus is an important subcortical target of the dorsal stream.** 

*Key Words:* **fMRI; brain function; BOLD response; dorsal stream; visuomotor.**

## INTRODUCTION

Accurate, visually guided movements require a series of integrative steps that transform retinal information into the appropriate motor output. Since the late 1960s two major visual pathways have been implicated in the spatial control of movement. As originally defined these two systems were hypothesized to consist of the retinal projection to the superior colliculus for localization of stimuli in space and the geniculostriate system for the identification of stimuli (*1*). Although this initial hypothesis was an oversimplification, the distinction between object identification and spatial localization—between ''what'' and ''where''—has persisted. Ungerleider and Mishkin (*2*) mapped this functional dichotomy onto two diverging projections or ''streams'' from the striate cortex. Based on experimental work in primates, these authors proposed that appreciation of an object's qualities and of its spatial location depends on the processing of different kinds of visual information. The former involves striate and extrastriate projections into the inferior temporal cortex, the ''ventral stream,'' and the latter striate and extrastriate projections into the posterior parietal cortex, the ''dorsal stream.'' Many recent positron emission tomography (PET) studies of the visual system are based on this two-cortical-stream theory, attempting to differentiate between object identification and object localization (*3–5*).

In Ungerleider and Mishkin's model, the distinction between the two pathways is based primarily on perceptual aspects of different stimulus attributes. Recently, the distinction between the ventral and dorsal streams has been approached rather differently. Milner and Goodale (*6, 7*) suggest that two different visual systems have evolved in the primate: (1) a visuomotor system associated with the dorsal stream that transforms visual information into action and (2) a perceptual system associated with the ventral system that is involved in off-line object recognition and is indirectly linked to action via cognitive processes. Within this conceptual framework, the underlying neural substrate for the dorsal stream involves not only the visual and parietal areas, but also the motor and premotor areas of the frontal cortex. The striate and extrastriate cortices connect to areas around the intraparietal sulcus and posterior parietal region; the posterior parietal region in turn connects reciprocally to the motor, premotor, and prefrontal cortices (*6–8*).



1090-7807/98 $25.00

The present study was undertaken to functionally map the activation occurring throughout the entire human brain during the performance of a visually guided motor task. While detailed information exists on the organization of the dorsal and ventral visual systems in the macaque monkey, less is known about corresponding areas in the human cerebral cortex. It is likely, however, that these general principles of organization are relevant for the human visuomotor system. Information on the human correlates has been obtained primarily from PET or functional magnetic resonance imaging (fMRI) studies. Most efforts have been directed at the perceptual aspects of vision. The visual pathways associated with the perception of color, movement shape, faces, and spatial location in the human extrastriate cortex have been investigated using PET in a variety of tasks (*5, 9–11*). Recent PET and fMRI studies have also investigated human cortical areas involved in the perception of visual motion (*12–18*). Activation during visually guided movements has been studied only over a limited set of brain areas (*19–23*).

In addition to the cerebral cortex, a visually guided motor task would also be expected to engage a variety of subcortical and cerebellar structures. Both lesion and electrophysiological data support a significant role for the cerebellum in visually guided movements (*24–26*). The cerebro–pontine projection is massive and includes many fibers from the extrastriate visual areas and the posterior parietal region (*27, 28*). The pulvinar is also expected to be part of the flow of visual and oculomotor information, receiving retinal (*29*), pretectal, and superior colliculus input (*30*) and in turn projecting to the dorsal and ventral streams (*31*).

Since its introduction (*32*), BOLD-based fMRI has been extensively used for identifying ''activated'' areas in the human brain (*33–37*). BOLD is sensitive to tissue deoxyhemoglobin content which is determined by the rates of oxygen consumption ($CMRO_2$) and cerebral blood flow (CBF). During increased local neuronal activity, it is generally thought that regional CBF increases without a commensurate increase in $CMRO_2$ (*38, 39*). The resultant decrease in regional deoxyhemoglobin generates susceptibility gradients across and near the luminal boundaries of blood vessels, increasing the signal in $T_2^*$- and/or $T_2$-weighted images. BOLD has been found to be consistent with CBF-based functional maps generated by PET (*40, 41*) or by perfusion-based MR imaging techniques (*42*).

In this study, the areas activated during a visually guided motor task were determined and compared to the activation produced by movements without visual guidance and the activation produced by eye movements without vision. Emphasis was placed on imaging the activation occurring throughout the whole brain and determining whether the activation was reproducibly observed across subjects. Preliminary accounts of some of these results have been presented in abstract form (*43, 44*).

## RESULTS

A three-dimensional reconstruction of the fMRI maps obtained from a single volunteer performing the visually guided two-step task is shown in Fig. 1. Four different views illustrate the task-related BOLD responses superimposed on the anatomical image of the brain after removal of the skull. The images are also presented with two different levels of opacity for the anatomic image shown in gray scale. On the top row, the anatomic images are opaque and only activation on the cortical surface is visible. The anatomic images in the lower row in Fig. 1 have been rendered partially translucent so that activation deep in the sulci can also be visualized, albeit with diminished intensity. Figures 1A and 1C reveal extensive activation bilaterally in the posterior parietal area and in the premotor cortex (part of Brodmann's area 6). Viewed from the top (Figs. 1A and 1C), unilateral activation in the left primary motor cortex (Brodmann's area 4) and in the left primary sensory cortex (Brodmann's area 3,1,2) contralateral to the moving hand as well as bilateral activation in the prefrontal cortex are clearly visible, especially in the partially translucent anatomic image. Cerebellar activation is evident in the views presented in Figs. 1B and 1D. The primary visual cortex (V1) does not appear activated, since the paradigm was designed with visual input in both the task and baseline periods.

When the 3D reconstruction is sliced in the coronal plane at the level of the posterior parietal region and the interior of the brain at the level of the cut is exposed (Fig. 2), the extent of the activation beyond the cortical surface becomes apparent. In particular, note the extensive bilateral activation in the occipito-temporal cortex in the region of the visual association areas. The location of this bilateral activation at the junction of Brodmann's area 19 and 37 just above the anterior commissure–posterior commissure (AC–PC) line and posterior to the ascending limb to the inferior temporal sulcus is very similar to that described for the human homologue of MT/V5 (*11, 16, 45*). In this coronal section bilateral activation in the intermediate and lateral regions of the cerebellum is evident. Although bilateral, the cerebellar activation was greater in the right anterior cerebellum, ipsilateral to the hand used to perform the task.

To examine the commonality of the activation pattern in different subjects, we warped all anatomical images and functional maps to the Talairach coordinate system as described under Experimental. Figure 3 displays 3D functional activation images from a single subject and for a group of six subjects as visualized from a left posterior and a right posterior view, respectively. Anatomical images are partially translucent to allow observation of sulci activity. The top row displays the functional map from a single subject subsequent to normalization and transformation of the brain into Talairach space (Figs. 3A and 3B); the dark line in these images identifies the central sulcus. The six-subject images

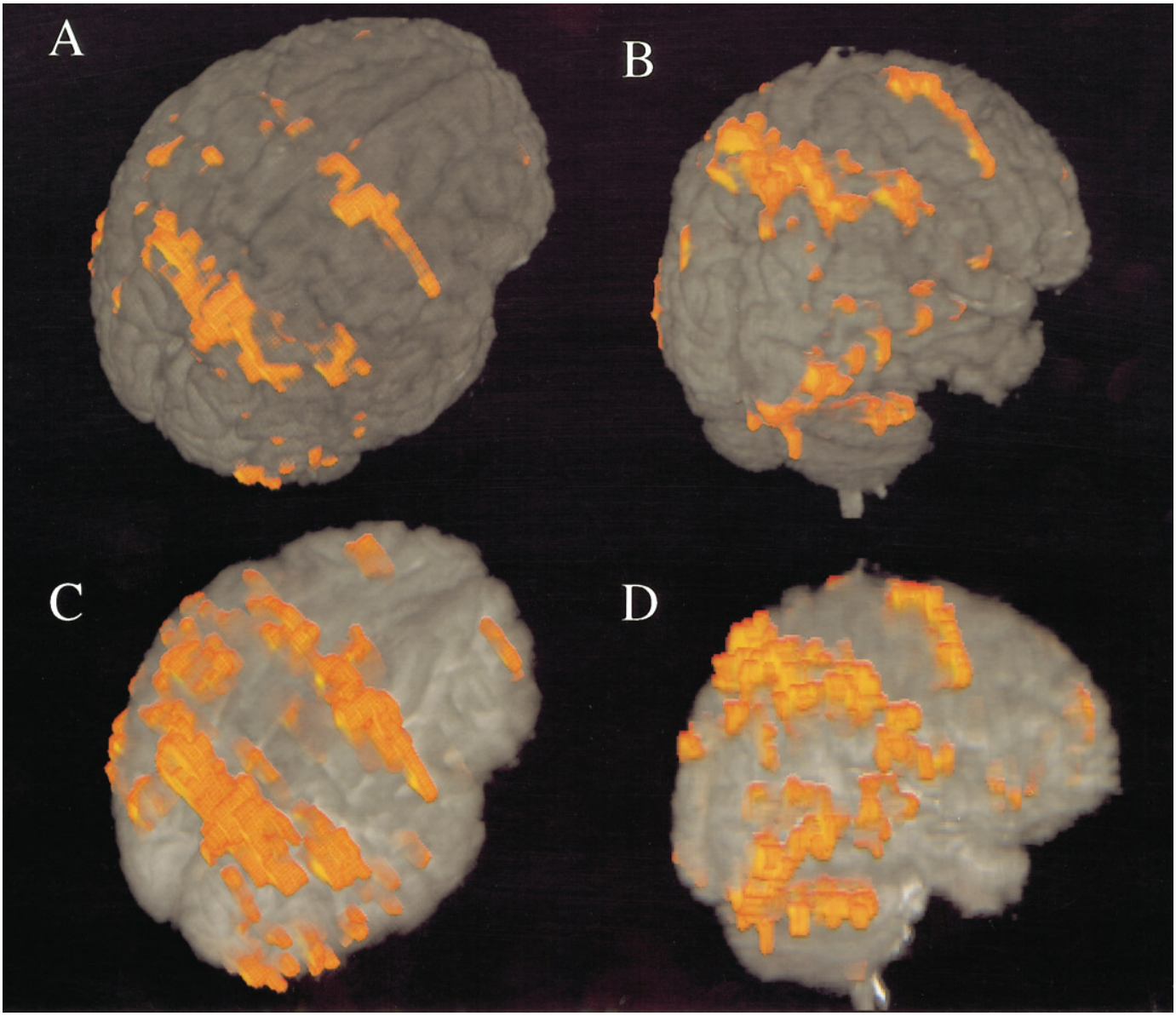


**FIG. 1.** A 3D reconstruction of the fMRI maps obtained from a single subject. Four different views illustrate the task-related, significant BOLD responses during the two-step task superimposed on the anatomical image of the brain after removal of the skull. The images are also presented with two different levels of opacity. (A) and (B) are less translucent than (C) and (D). The 3D reconstructions are shown in a standard anatomical view (right side of image is right side of the brain).

(Figs. 3C and 3D) display areas of activation common to four or more of the six subjects (i.e., minimum of four out of six subjects must have a pixel with a significant BOLD effect for the pixel to be considered ''activated'' in these composite maps). With respect to these composite images, it must be stressed that no existing normalization procedure

**FIG. 2.** The 3D reconstruction of the brain sliced in the coronal plane at the level of the posterior parietal region. The inner structures of the brain at the plane of the cut are exposed and the extent of the activation beyond the cortical surface becomes apparent. Same subject as shown in Fig. 1.

**FIG. 3.** To examine the commonality of the activation pattern in different subjects, the anatomical and functional maps were warped to the Talairach coordinate system. Anatomical images are partially translucent to allow observation of sulcul activity. The top row displays the functional map from a single subject (A, B); the dark line in these images identifies the central sulcus. The composite maps of six subjects (C, D) display areas of activation common to four *or more* of the six subjects (i.e., minimum of four out of six subjects must have a 8-pixel cluster activated to be included in these maps). Within this restriction, the activation patterns obtained for a single subject and for a group of six subjects are in good agreement.

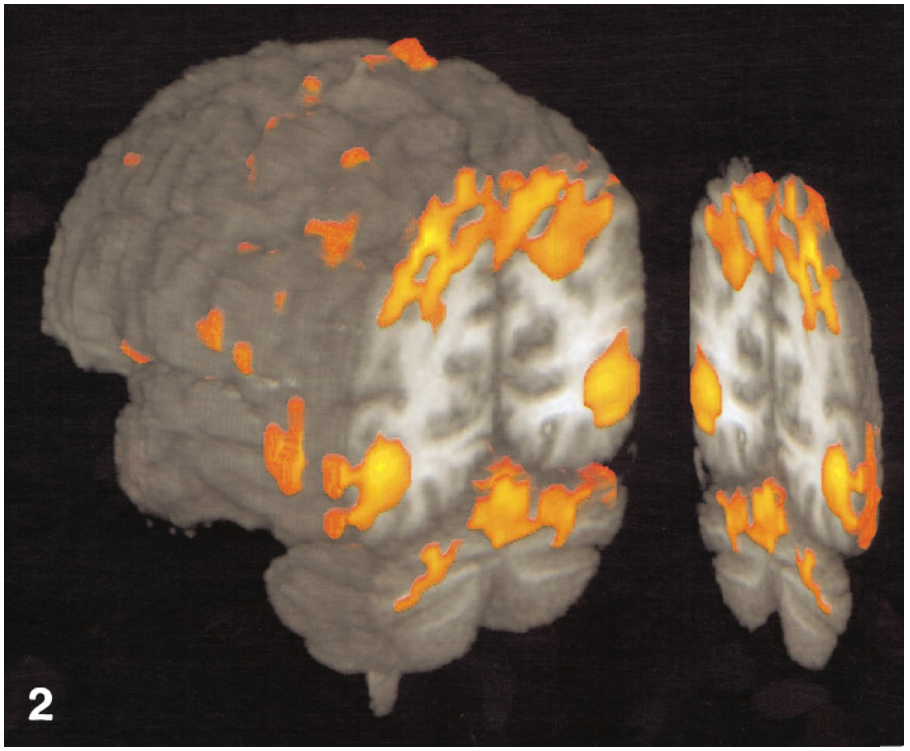
2

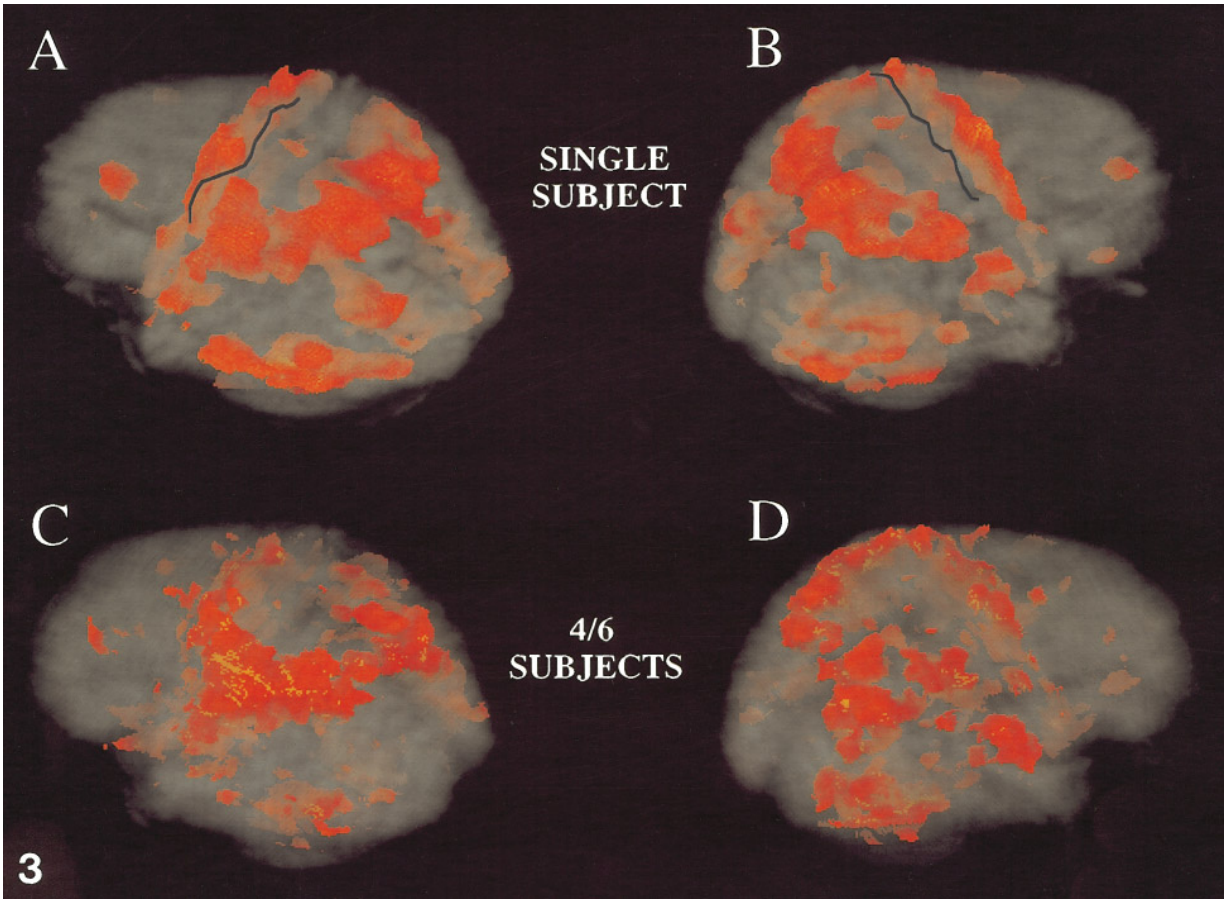
A
B
SINGLE
SUBJECT
C
D
4/6
SUBJECTS
3

yields exact agreement of spatial locations among different individual brains. The same anatomical region may be as much as 1 cm apart for different individuals in Talairach space. Thus, the effective spatial specificity of these composite maps are in the range of several millimeters to one centimeter. Within this restriction, the activation patterns obtained for a single subject and for a group of six subjects are in agreement. Both reveal the extensive bilateral activation of the posterior parietal area and the premotor cortex, the unilateral primary motor and sensory cortex activation, and the activation that follows the central sulcus along the lateral surface of the brain bilaterally toward the inferior frontal gyrus. Activation in extrastriate visual areas (Brodmann's area 18 and 19) is evident in the single and group maps.

Table 1 lists the activated cortical areas, subcortical nuclei, and cerebellar structures displayed in the composite images illustrated in Figs. 3C and D. Table 1 includes the name of the activated anatomical structure, its occurrence in the left or right hemisphere, the Talairach coordinates of the center of mass of the activation within this anatomical structure, and the Brodmann's area. Furthermore, the number of activated pixels, the slice numbers (see Fig. 4) displaying the activated structures, and the appearance in four, five, or six out of six subjects are listed. These activated areas, identified from the six-subject composite functional maps, are also depicted in coronal slices in Fig. 4. Irrespective of the specific colors (the significance of the different colors in Fig. 4 is discussed later), the colored areas depict activation common to at least four out of six subjects. Not all slices are illustrated in Fig. 4 because of space considerations. Therefore, the areas of activation listed in Table 1 do not necessarily all appear in these images.

As listed in Table 1, in six out of six subjects activation occurred in the superior frontal gyrus bilaterally (Fig. 4: Brodmann's area 6, slices 11 and 12 in the right hemisphere, 12 and 13 in the left hemisphere). The middle frontal gyrus (Brodmann's area 8) was bilaterally activated (in the left hemisphere in four out of six subjects, slices 17 and 18; and in the right hemisphere in five out of six subjects, slices 16 and 18). The inferior frontal gyrus (Brodmann's area 44, 45) was activated bilaterally in five out of six subjects (slices 16 to 18 in the right hemisphere and slice 16 in the left hemisphere). A positive BOLD effect was detected in the left precentral gyrus (Brodmann's area 4) in all subjects (slices 10–12) in an area that contains wrist, hand, and finger representations. There was also bilateral activation more laterally in Brodmann's area 4 in a region consistent with the face and oculomotor representations and in the region of the insula (slices 14 and 15, five out of six subjects on the right, in slice 14 in the left hemisphere in all subjects). The cingulate gyrus was activated bilaterally in all subjects (slices 9, 11–14).

The parietal lobe was extensively activated, including the superior parietal lobule (Brodmann's area 5, 7) in both hemispheres (slices 1–8 in the right hemisphere, slices 2–9 in the left hemisphere). The left superior parietal lobule was activated in all subjects, the right superior parietal lobe in five out of six subjects. The inferior parietal lobule (Brodmann's area 40) was activated bilaterally, but with a left hemispheric dominance (slices 5–10 in the left hemisphere in all subjects, slices 7–10 in the right hemisphere in five subjects). In slices 5 and 6 activation of the parietal medial wall areas (precuneus) in the right hemisphere was evident in five subjects. Activation of the left postcentral gyrus can be appreciated in slices 7–10, and there was some bilateral activation in somatosensory cortex in five subjects (slices 10 and 11). The cingulate gyrus (Brodmann's area 31/23) was also activated bilaterally (slices 9–13 on the left, 9 and 11–14 on the right) but with left hemispheric dominance in all subjects.

In the temporal lobe activation in the inferior temporal gyrus (Brodmann's area 37) occurred bilaterally in all six subjects in slices 3–6. In the right middle temporal gyrus (Brodmann's area 21, 39) activation is evident in slices 3 and 6 to 8 for five subjects. The activation in the left middle temporal gyrus (Brodmann's area 21, 39) is shown in slices 3, 4, and 7 in five subjects. The posterior part of the superior temporal gyrus was activated (Brodmann's area 22, slices 5–10 on the right in five subjects, slices 6–10 on the left in all six subjects). The insula (Brodmann's areas 22, 41–43, slices 11–15) and the inferior temporal gyrus (Brodmann's area 37, slices 3–6 in all six) were also activated bilaterally.

Positive BOLD effects in the occipital lobe included bilateral activation in the middle occipital gyrus in five subjects (Brodmann's area 18 and 19, slices 0–2). The superior and inferior occipital gyri, also part of Brodmann's area 18 and 19, were activated in the right hemisphere in five out of six subjects (slices 1 and 2). In addition, there was bilateral activation of the fusiform gyrus in five out of six subjects (Brodmann's area 19, slices 3–6) and the cuneus (Brodmann's area 19, slices 2 and 3).

Subcortically, several major motor systems and pathways were activated. Activation in the thalamic nuclei occurred bilaterally in the pulvinar (slices 10 and 11 in the left hemisphere in all subjects, slice 11 in the right hemisphere in five subjects), bilaterally in the lateral posterior nucleus (slice 11 in five subjects), in the ventral posterolateral and ventral posteromedial (left hemisphere, slice 11 in four subjects) as well as in the ventral lateral nuclei (left hemisphere, slice 12 in four subjects). Activation in the basal ganglia included the left putamen (slices 12 and 13) and the left globus pallidus (slices 12 and 13).

Cerebellar activation occurred in the vermis (slices 2–6) in all subjects. The right intermediate region of the cortex (slice 3–8) as well as the lateral right hemisphere (slices 3, 5–8) were activated in all subjects. Activation also occurred in the left intermediate (slices 3–5) and lateral (slices 3–7) cerebellar hemisphere in five subjects but the activa-

**TABLE 1**

**The Activated Cortical Areas, Subcortical Nuclei, and Cerebellar Structures Displayed in the Composite Functional Maps in Fig. 4**

| Structure | Side | Tailarach | Brod | Pixels | Slice | 4 of 6 | 5 of 6 | 6 of 6 |
|---|---|---|---|---|---|---|---|---|
| Occipital Lobe | | | | | | | | |
| Fusiform Gyr | R | −35.7, −59.0, 13.4; rbG10 | 19 | 428 | 3–6 | 1 | 1 | 0 |
| Fusiform Gyr | L | 40.7, −59.0, 13.4; lcG10 | 19 | 116 | 4–6 | 1 | 1 | 0 |
| Lingual Gyr | R | −17.8, −86.4, 14.5; rbl10 | 18 | 37 | 0 | 1 | 0 | 0 |
| Inferior Occ Gyr | R | −34.0, −79.6, 11.4; rbH10 | 18 | 204 | 1, 2 | 1 | 1 | 0 |
| Middle Occ Gyr | R | −32.5, −79.4, −0.49; rbH8 | 19, 18 | 727 | 0–2 | 1 | 1 | 0 |
| Middle Occ Gyr | L | 37.1, −76.3, −0.02; lcH8 | 19, 18 | 264 | 0–2 | 1 | 1 | 0 |
| Superior Occ Gyr | R | −25.4, −77.0, −24.3; rbH6 | 19 | 195 | 1, 2 | 1 | 1 | 0 |
| Cuneus | R | −3.5, −72.5, −41.0; raH4 | 19 | 32 | 2, 3 | 1 | 0 | 0 |
| Cuneus | L | 0.0, −72.5, 39.4; laH4 | 19 | 10 | 2, 3 | 1 | 0 | 0 |
| Parietal Lobe | | | | | | | | |
| Precuneus | R | −12.1, −51.6, −44.9; raG4 | 7 | 32 | 5, 6 | 1 | 1 | 0 |
| Sup Par Lobule | R | −23.8, −60.0, −38.9; rbG_H4 | 7, 5 | 2814 | 1–8 | 1 | 1 | 0 |
| Sup Par Lobule | L | 28.1, −54.4, −43.1; lbG4 | 7, 5 | 3002 | 2–9 | 1 | 1 | 1 |
| Inf Par Lobule | R | −50.6, −37.1, −30.5; rcF5 | 40 | 371 | 7–10 | 1 | 1 | 0 |
| Inf Par Lobule | L | 41.1, −43.6, −33.8; lcG5 | 40 | 1990 | 5–10 | 1 | 1 | 1 |
| Postcent Gyr | R ant | −40.1, −22.8, −49.1; rcE33 | 1, 2, 3 | 113 | 11 | 1 | 1 | 0 |
| Postcent Gyr | L ant | 36.5, −26.4, −43.5; lcF4 | 1, 2, 3 | 154 | 10, 11 | 1 | 1 | 0 |
| Postcent Gyr | L post | 32.1, −37.0, −54.1; lbF3 | 1, 2, 3 | 490 | 7–10 | 1 | 1 | 0 |
| Frontal Lobe | | | | | | | | |
| Precent Gyr | R | −22.4, −22.8, −49.1; rb$E_3$3 | 4 | 172 | 11 | 1 | 1 | 0 |
| Precent Gyr | L | 27.0, −21.7, −53.7; lb$E_3$3 | 4 | 414 | 10–12 | 1 | 1 | 1 |
| Sup Front Gyr | R | −20.6, −18.7, −49.9; ra$E_3$3 | 6 | 631 | 11, 12 | 1 | 1 | 1 |
| Sup Front Gyr | L | 18.1, −15.6, −51.4; la$E_3$3 | 6 | 489 | 12, 13 | 1 | 1 | 1 |
| Mid Front Gyr | R | −26.1, 11.5, −30.1; rbD5 | 8 | 87 | 16, 18 | 1 | 1 | 0 |
| Mid Front Gyr | L | 28.7, 16.0, −29.1; lbC5 | 8 | 90 | 17, 18 | 1 | 0 | 0 |
| Inf Front Gyr | R | −31.2, 11.7, −0.81; rbD8 | 44, 45 | 336 | 16–18 | 1 | 1 | 0 |
| Inf Front Gyr | L | 39.1, 7.05, −0.89; lcD8 | 44, 45 | 96 | 16 | 1 | 1 | 0 |
| Medial Front Gyr | L | 5.6, −20.0, −53.0; la$E_3$3 | 6 | 555 | 11, 12 | 1 | 1 | 0 |
| Medial Front Gyr | R | −4.9, −16.4, −51.7; ra$E_3$3 | 6 | 304 | 11, 12 | 1 | 1 | 0 |
| Limbic Lobe | | | | | | | | |
| Cing Gyr | R | −5.4, −13.0, −40.4; ra$E_2$4 | 31, 32, 23, 24 | 640 | 9, 11–14 | 1 | 1 | 1 |
| Cing Gyr | L | 8.7, −20.1, −41.3; la$E_3$4 | 31, 32, 23, 24 | 1159 | 9–13 | 1 | 1 | 1 |
| Temporal Lobe | | | | | | | | |
| Inf Temp Gyr | R | −40.4, −62.9, 0.65; rcH9 | 37 | 739 | 3–6 | 1 | 1 | 1 |
| Inf Temp Gyr | L | 40.6, −62.5, 0.51; rcH9 | 37 | 870 | 3–6 | 1 | 1 | 1 |
| Mid Temp Gyr | R | −43.8, −50.0, 0.59; rcG8 | 21, 39 | 599 | 3, 6–8 | 1 | 1 | 0 |
| Mid Temp Gyr | L | 44.3, −63.8, −0.34; lcH8 | 21, 39 | 265 | 3, 4, 7 | 1 | 1 | 0 |
| Sup Temp Gyr | R | −50.5, −42.2, −16.9; rcG7 | 22 | 904 | 5–10 | 1 | 1 | 0 |
| Sup Temp Gyr | L | 45.4, −37.6, −15.4; lcF7 | 22 | 1039 | 6–10 | 1 | 1 | 1 |
| Insula | R | −35.6, −2.4, −5.9; rc$E_1$8 | 4, 6, 22, 41–43 | 538 | 13–15 | 1 | 1 | 0 |
| Insula | L | 41.0, −11.7, −0.6; lc$E_2$8 | 4, 6, 22, 41–43 | 1241 | 11–15 | 1 | 1 | 1 |
| Thalamus | | | | | | | | |
| Pulvinar | R | −11.5, −28.6, −7.3; raF8 | | 116 | 11 | 1 | 1 | 0 |
| Pulvinar | L | 16.3, −28.6, −5.1; laF8 | | 595 | 10, 11 | 1 | 1 | 1 |
| Ventral posterior/lateral medial n. | L | 12.8, −22.8, −4.1; laE38 | | 215 | 11 | 1 | 0 | 0 |
| Lateral posterior n. | R | −11.7, −22.8, −10.1; raE37 | | 60 | 11 | 1 | 1 | 0 |
| Lateral posterior n. | L | 18.2, −22.8, −12.6; laE37 | | 161 | 11 | 1 | 1 | 0 |
| Ventral lateral n. | L | 9.6, −17.1, −10.5; laE37 | | 11 | 12 | 1 | 0 | 0 |
| Basal Ganglia | | | | | | | | |
| Putamen & globus pallidus | L | 20.0, −14.2, −8.1; lbE38 | | 157 | 12, 13 | 1 | 1 | 1 |
| Cerebellum | | | | | | | | |
| Dentate n. | R | −16.0, −57.5, 37.5; raG12 | | 38 | 5 | 1 | 1 | 0 |
| Lateral | R | −20.0, −49.9, 25.2; rbG11 | | 891 | 3, 5–8 | 1 | 1 | 1 |
| Lateral | L | 30.6, −55.3, 27.5; lbG11 | | 630 | 3–7 | 1 | 1 | 0 |
| Intermediate | R | −8.0, −58.0, 22.0; raG11 | | 1129 | 3–8 | 1 | 1 | 1 |
| Intermediate | L | 5.2, −63.5, 21.7; laG11 | | 391 | 3–5 | 1 | 0 | 0 |
| Vermis | | 0.01, −61.0, 21.0; laH11 | | 922 | 2–6 | 1 | 1 | 1 |

*Note.* Includes the side of activation, the Talairach coordinates of the center of mass of the activation for each structure, Brodmann's area if a cerebral cortical structure, the number of activated pixels, the slice numbers, and whether the activation was present in four, five, or six out of six subjects.

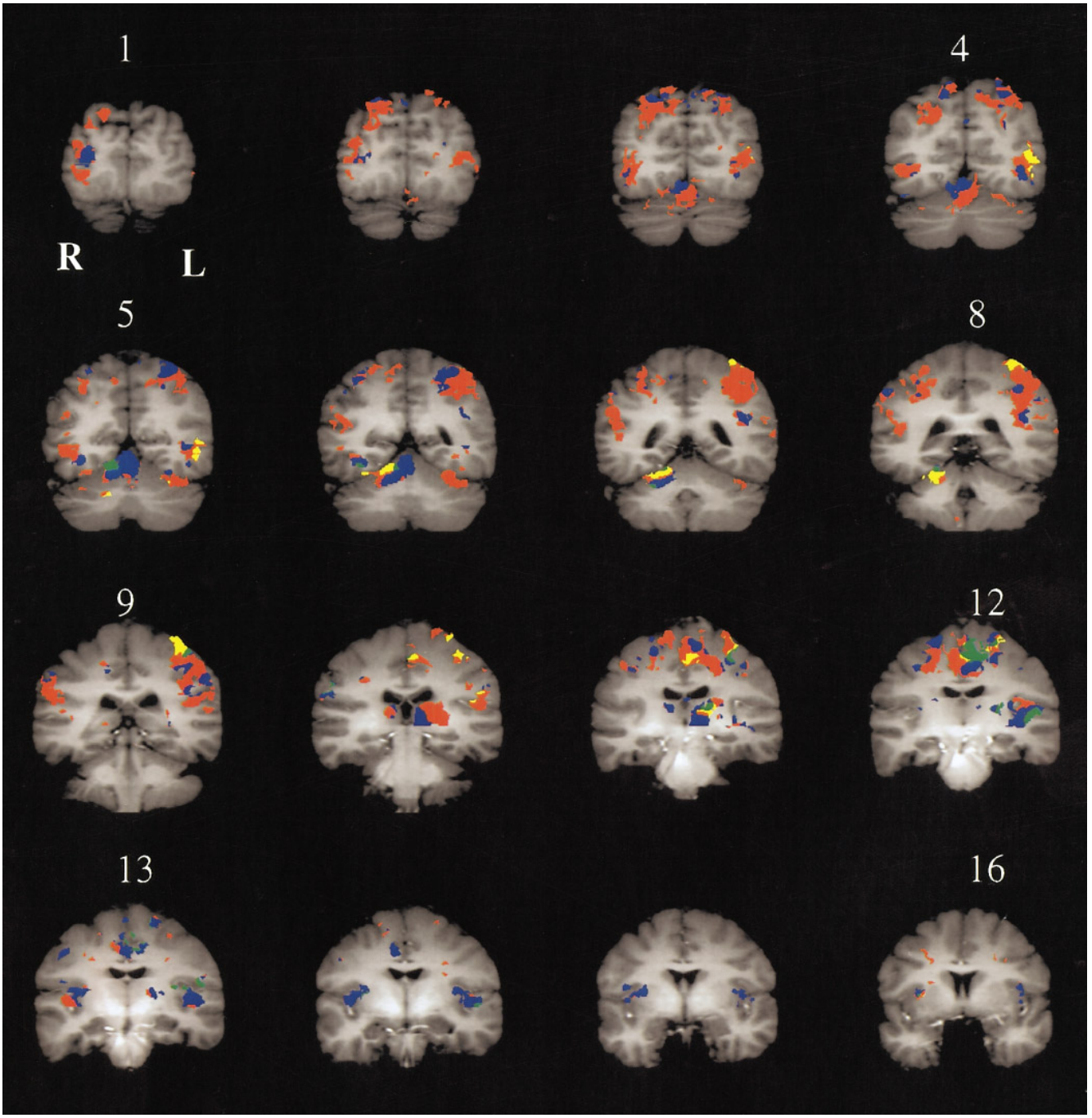


**FIG. 4.** The color code in the coronal slices displayed in Fig. 5 identifies areas that were activated by the visually guided two-step task as well as one of the two other tasks performed, to delineate regions that may be accounted for by eye movements and hand/wrist directed joy stick movements without visual guidance. Areas in *blue* identify regions that were activated both in the eye movement task that overlapped with the activation in the two-step task. *Yellow* identifies regions common to the hand/wrist directed joystick movements and the two-step task. *Green* identifies regions activated in all three tasks. Remaining activation not accounted for by either the joystick movement and/or the eye movement is depicted in *red*. Coronal slices are shown in standard radiographic format (right side of image is left side of the brain).

tion on the right was more extensive. As shown in slice 5, activation of the right dentate nucleus occurred in four subjects. The left dentate was activated in only three subjects (data not shown).

The color code in the coronal slices displayed in Fig. 4 identifies the areas that were activated by the visually guided two-step task as well as one of the two other tasks performed to delineate regions that may be accounted for by eye move-

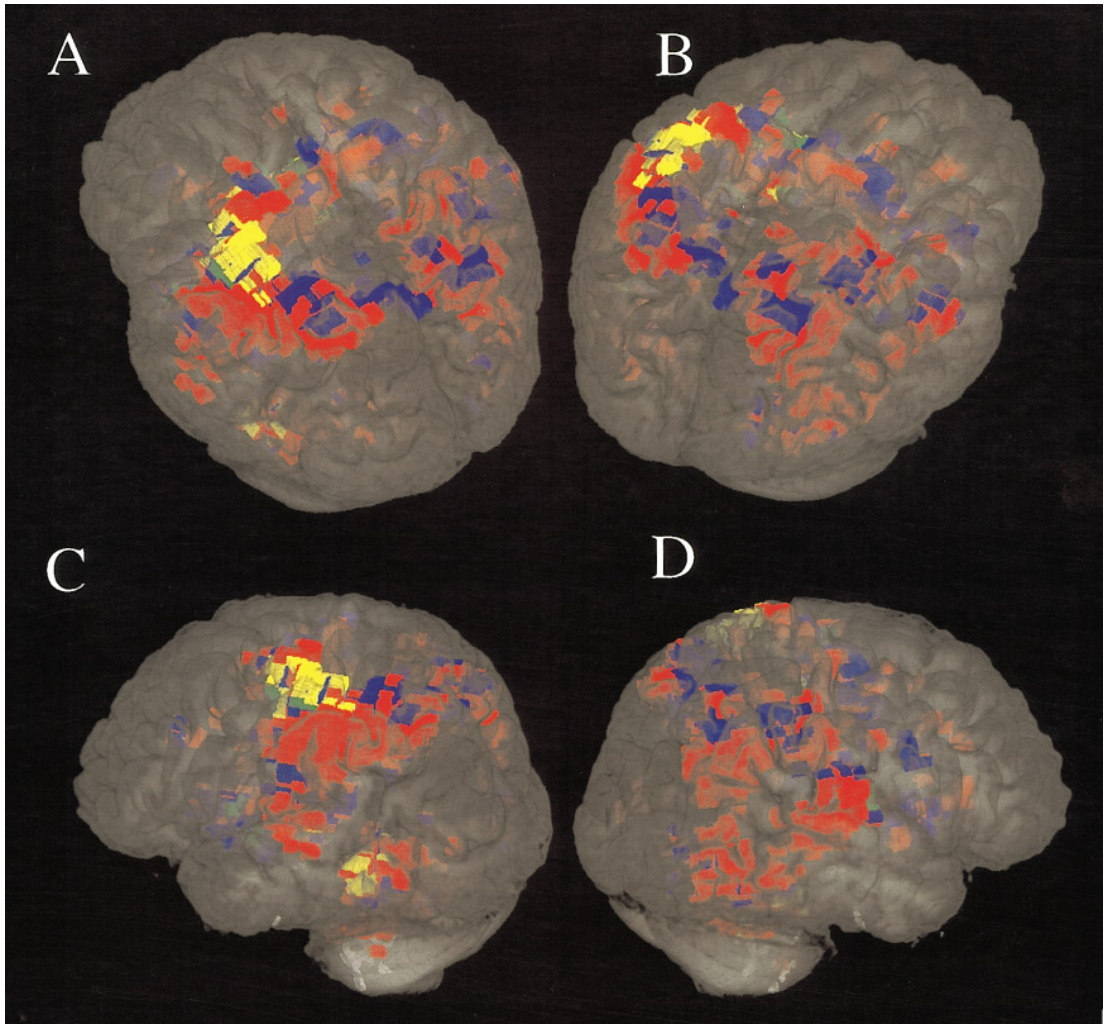


**FIG. 5.** Three-dimensional reconstruction of the functional maps viewed from a left oblique (A), right oblique (B), and left (C) and right (D) lateral perspective displaying the activation pattern shown in Fig. 4. The same color code is used.

ments and hand/wrist movements without visual guidance. Areas in blue were activated both in the eye movement task and in the two-step task. Yellow color identifies regions common to the hand/wrist joystick task and the two-step task. Green identifies regions activated in all three tasks. Regions activated by the two-step task but not by either the hand or the eye movement task are depicted in red. Figure 5 displays these areas with the same color code in a three-dimensional view. All areas in color taken together represent the activation due to the visually guided two-step tracking task. Activation by the eye movement and hand movement tasks that did not overlap the two-step task is not shown. The overlap of activation between the hand movement without visual guidance and the visually guided two-step task (color code yellow and green) included the contralateral primary motor cortex (Brodmann's area 4, slices 10–12), the primary somatosensory cortex (slices 7–10), the premotor cortex, and the medial wall motor areas including the cingulate gyrus (slices 10–13). As expected, the cerebellum was activated in the hand movement and the two-step tasks in the right intermediate cortex (yellow and green areas in the cerebellum, slices 5–8). The right dentate nucleus shows common areas of activation (yellow color, slice 5) for the hand and two-step tasks. The thalamic relay nuclei between motor and premotor areas, and the cerebellum include the ventrolateral and ventral anterior nuclei; their activation appears predominantly in slice 11. Putamen and globus pallidus were also activated (slices 12 and 13) in the hand and two-step tasks.

Specific activation due to eye movements, which included both smooth pursuit as well as saccades during the two-step task (blue and green color code), was expected to and did include the areas around the precentral sulcus bilaterally (slices 11 and 12), medial wall motor areas including the cingulate gyrus and the medial frontal gyrus (slices 11–14). The superior frontal gyrus (Brodmann's area 6, supplemen-

tary eye fields) was activated bilaterally (slices 12 and 13). Common activation due to eye movement and two-step tasks was found in the rostral insular area (slices 12–15) and in the inferior frontal gyrus (Brodmann's area 44, slice 16). The coronal slices demonstrate a positive BOLD response in the cerebellar vermis area (slices 3–6) common to the eye movement and the two-step tasks, although activation with the latter was more extensive (slices 3, 4). Additional areas of common activation between the eye movement and the two-step visuomotor tracking tasks included the superior parietal lobule bilaterally (slices 3–6), some bilateral activation in the inferior parietal lobule (slices 8 and 9), and activation at the junction of medial and inferior temporal lobe (area MT in slices 3–5). Eye movement resulted in activation in the bilateral pulvinar nucleus of the thalamus (slices 10 and 11) and in the basal ganglia (slice 12). Cerebral cortical regions activated primarily by the two-step task and not the other two tasks (red color code) included large areas of the extrastriate visual cortices, MT, and the posterior parietal region (superior and inferior parietal lobe). Subcortical areas activated primarily by the two-step included the lateral pulvinar, the lateral cerebellum, and cerebellar vermis.

## DISCUSSION AND CONCLUSIONS

Our two-step task required of the subject a complex interplay of vision and movements including: (1) visual recognition of the appearance of a target, (2) saccadic eye movements to the target to initiate a hand movement to the correct position in space, (3) monitoring the position of the cursor on the screen, (4) recognition of and responding to the displacement of the target, and (5) using this information to move and accurately place the cursor within the new target. Furthermore, the task required coordinate transformations between information on a vertically placed screen and the hand movements at the joystick. The large number of cortical and subcortical structures activated suggests that a variety of networks participate in visually guided movements. In this discussion, we emphasize the possible roles of the dorsal stream, cerebellum, and thalamus.

### *Activation of the Dorsal Stream*

Milner and Goodale have hypothesized that the dorsal stream plays a major role in transforming visual information into movement (*6, 7*). The present functional mapping results support this concept. Prominent and common to most subjects in the activation maps were the bilateral activation of: (1) extrastriate visual cortices (Brodmann's area 18 and 19), (2) region at the border of the inferior temporal and occipital lobules (the human analog of MT), (3) posterior parietal region including Brodmann's areas 7a and 39, (4) the premotor cortex, and (5) contralateral activation of the primary motor cortex.

The activation of the posterior parietal cortex is consistent with it being a major node of the dorsal stream. There are a number of different routes by which the posterior parietal region receives striate and extrastriate visual signals (*46*). One set of information arrives via area MT (middle temporal area), which receives input from V1 and V2. Projections from MT reach parietal area 7a via MST (medial superior temporal area) and FST (fundus of superior temporal sulcus) (*47*). Additional routes of visual input from areas V2 and V3 reach the posterior parietal cortex via V3A and via the parieto–occipital (PO) area.

The posterior parietal cortex is hypothesized to play a major role in visuomotor transformations. In humans, damage in and near the superior parietal region causes various visuomotor disorders, including optic ataxia. There is a convergence of visual, somatosensory, and movement signals within the posterior parietal lobule. In the primate, the discharge of cells within the various subdivisions cannot easily be characterized as sensory or motor (*48, 49*). For example, cells in the medial intraparietal (MIP) area are responsive to visual and somatosensory stimuli (*49*) and the direction of limb movement and the position of the arm in space (*19*). More dorsally located area 5 cells are also highly modulated by movement direction and limb position (*8, 50*). A gradient of activities has been reported across the superior parietal lobule, with cells in the more ventral and intermediate sulci more frequently related to signal and set-related activities than cells in the more dorsal area 5 which are more frequently modulated by movement (*8, 50*). Cells in area 7a and the lateral intraparietal area have gaze-dependent responses including sensitivity to the position of the eyes relative to the head and the head relative to the body (*51, 52*).

This convergence of sensory and motor signals projects into the frontal motor areas, completing the circuitry needed for the visual guidance of movements. Dorsal area 5d projects to the primary motor cortex, and MIP projects to the dorsal premotor cortex and to the border between the dorsal premotor cortex and primary motor cortex. Posterior parietal areas 7m and the medial dorsal parietal area project mainly to the dorsal premotor cortex with reciprocal connections from the premotor cortex and primary motor cortex back to the superior parietal lobule. The PO projects to PMd and more anteriorly in the frontal cortex. It should be pointed out that the human analogue of the posterior parietal cortex in the monkey involves structures such as the superior part of the angular gyrus and the supramarginal gyrus (Brodmann's area 39 and 40) (*4, 7*) which were also extensively activated by the two-step task. Therefore, the extensive and bilateral activation of the posterior parietal cortex and the premotor and motor cortices is compelling evidence for the dorsal stream's role in visuomotor behavior (*7*).

One of the prominent areas of activation was at the border of the temporal and occipital cortices. This region was bilaterally activated in most subjects in the two-step task (see

Table 1). In addition to the visual target motion on the screen, in this paradigm the subjects must monitor the movement of the cursor, and it is also likely that the subjects used pursuit eye movements (*53*). In the nonhuman primate, neurons within area MT are highly sensitive to the direction and velocity of the visual stimulus (*54*). Pursuit tracking of a moving target activates cells in MT and MST, two areas primarily responsible for object motion coding. In PET (*11, 45, 53*) as well as in recent f MRI studies (*16*) the human homologue of area MT was shown to lie at the tip of the ascending limb of the inferior temporal sulcus at the border between the temporal and occipital lobes. Furthermore, there is evidence from human PET studies that the motion sensitive areas in the caudal superior temporal sulcus interact with the parietal cortex in the analysis of complex motion patterns (*13, 55*).

### *Activation of the Parietal Lobe Due to Nonmotor Task Features*

Two nonmotor features of the task may have contributed to the activation patterns observed in this study. Two different cortical systems are activated during visual perception of faces and locations (*4*). Face matching has been shown to selectively increase rCBF in the fusiform gyrus in the occipital and occipitotemporal cortex bilaterally and in the right dorsal premotor cortex. The dorsal parietal region is also activated during visual spatial matching (*5*). The right dorsal inferior parietal lobule was more activated during spatial matching than object matching, whereas bilateral ventral occipitotemporal regions were more activated during the object matching. The authors interpreted the right parietal region activation during the spatial matching task as subserving the computation of the required coordinate transformations for visuomotor control. During the matching of spatial location in connection with visual memory, unilateral right inferior parietal activation also has been observed (*5, 56*).

Shifting visuospatial attention in the absence of movement also increases cerebral blood flow in the superior parietal lobule (*57*), and patients with lesions in this region have considerable problems in shifting attention to the contralateral visual field in a covert orienting task (*58*). The superior parietal region in the human may be the functional homologue of area 7a in monkeys and involved in not only visuomotor control, but also in mediating spatial attention. Since the two-step task required attention to the spatial aspects of the cursor and target placement on the screen as well as shifting and maintaining spatial attention, these factors may have contributed to parietal activation observed.

### *Subcortical Activation*

The cortical visuomotor circuitry is highly interconnected with subcortical structures involved in visuomotor control (*25, 59–61*). The cortico–ponto–cerebellar projection is one of the largest in the brain, arising from areas 4, 6, and 8, frontal eye fields, somatosensory cortex, posterior parietal lobule, and cingulate gyrus (*28*). One of the main targets of the cortico–ponto–cerebellar projection is the dorsolateral pontine nuclei (DLPN) which in turn projects to the cerebellum. There are dense projections from the cortical areas of the dorsal stream, whereas there are very sparse or absent projections from cortical areas of the ventral stream. The dorsal stream contributes fibers from the posterior parietal complex (areas 5 and 7, LIP, and PO), primary and premotor areas (4, 6), as well as from the frontal eye field region and extrastriate areas including areas MST and MT (*28*). All these cortical areas were activated in the two-step task in at least four out of six subjects (Fig. 5 and Table 1).

Pontocerebellar fibers then connect mainly to areas in the lateral cerebellum which was also activated in the two-step task (Fig. 4 and Table 1). In three out of six subjects we observed activation in pontine nuclei in the left brainstem (data not shown). These pontine nuclei are closely linked with the cerebellum, and these pontocerebellar circuits have been implicated in visuomotor control (*25, 61*). We observed cerebellar activation bilaterally in the vermis, as well as in the mediolateral and lateral zones. The lateral activation was not present during the eye and limb movement tasks. These findings would reinforce the view that the dorsal stream interacts with subcortical visuomotor networks. Interestingly similar projections are apparently completely absent from the inferotemporal cortex (*24, 62*). The dentate nucleus and the nuclei of the motor thalamus were activated, the major output pathway of the lateral cerebellum that targets the motor and premotor areas.

Two additional subcortical areas were activated. The first is the putamen and caudate nucleus (*63*). Both receive projections from the posterior parietal and frontal motor areas and are involved in the control of reaching (*64*). The second is the pulvinar, one of the more important sources of extrageniculate input to the cerebral cortex. The pulvinar receives input from the superior colliculus (*65*) and pretectal areas (*66*) and directly from the retina (*29*). In the absence of the striate cortex, many of the cells in MT receive input about stimulus motion that originates in the superior colliculus via the pulvinar (*67*). In turn, the pulvinar sends information directly to the dorsal and ventral streams. These projections to the pulvinar are segregated with the medial pulvinar linked to the dorsal stream and the lateral pulvinar linked with the ventral stream (*31, 62*). The medial subdivision of the nucleus is mainly concerned with oculomotor function. Although no medial versus lateral division of labor was evident in the present imaging results, it should be stressed that there was no explicit attempt to independently activate dorsal and ventral streams. The pulvinar may be specifically engaged in tasks requiring attention to visually important spatial information. The lateral pulvinar is coactivated with the posterior parietal cortex in a task involving spatial attention

(*68, 69*). Neurons in the posterior parietal cortex and the lateral pulvinar show a selective enhancement of a visual response when the animal covertly attends to a stimulus location (*70*). Therefore, it is interesting that the pulvinar was extensively activated in the two-step task but not during the hand or eye movement only tasks.

## EXPERIMENTAL

### *Behavioral Paradigms*

Nine right-handed volunteers (mean age 31 years) participated in this study. All subjects gave written informed consent and the studies were approved by the institutional review board of the University of Minnesota Medical School. Three different sets of experiments were conducted. In the first set, six healthy subjects were studied with $T_2^*$-weighted BOLD contrast images while performing a two-step, visually guided task. With their right hands subjects used a joystick that was held in their lap, moving a crosshair-shaped cursor projected onto a rear projection screen at the end of the bore of the scanner (*23*). The subjects viewed the screen through a pair of prism glasses. Computer-generated and -controlled behavioral paradigms were projected onto the screen using a high wattage, overhead projection system. The task was designed to require continual visual attention and was a modification of a center-out design (*71, 72*). Two sets of eight targets were arranged in two concentric circles (0° to 360° at 45° intervals) at two different distances around a center start box. The individual targets in each circle were aligned along the same radial directions. The targets positioned around the inner circle were one-half the distance to the targets positioned around the outer circle.

A trial was initiated by the appearance of the center box and the subject was first required to move to and hold the cursor in the start box for a pseudorandomized period of 500–1000 ms. Next, one of the eight short distance targets appeared pseudorandomly and the subject was required to move to that target. On placing the cursor in the target, the target was extinguished and the longer distance target along the same direction was illuminated and the subject was to move to this second target. The subject was required to hold the cursor within the second target for 750 ms. The subject had 2 s to complete the entire sequence, otherwise the trial was aborted. Failure to complete any step of the sequence also resulted in aborting the trial. For either a completed or failed trial, the center box reappeared and the task sequence was repeated. All subjects practiced the paradigm while in the bore of the scanner prior to the actual scanning. During the baseline (i.e., rest) periods, the volunteers laid motionless looking at a colored box on a lighted screen.

The second and third sets of experiments were designed to assess the contributions to the activation maps from the movement of the joystick or eye movements, respectively, without the visual input. Both sets of experiments were performed with the room completely dark and the subject's eyes were closed during both the baseline and task periods. In the hand movement task, six volunteers were asked to move the joystick with their right hand and wrist during the task period and relax during the baseline period. In the eye movement task, four subjects were asked to relax and not move their eyes during the baseline period and to start moving their eyes between right and left sides. For both tasks the movements were paced at 1.5 s intervals by a brief auditory cue. The cue was present during both the baseline and task periods to remove the auditory contribution. Finally, we controlled for effects of selective attention during the performance of the tracking task by analyzing experiments in which the volunteers performed with a minimum success rate of 75%.

### *Imaging Protocols and Analyses*

Studies were performed on a 4-T whole-body magnet with a 1.25 m diameter horizontal bore (Siemens/Erlangen, Germany) interfaced to a Varian console (Palo Alto, CA). The magnet was equipped with a head gradient coil insert operating at a gradient strength of 30 mT/m and a slew rate of 150 mT/m/s along all three axes. A homogeneous quadrature head birdcage RF coil was used for RF transmission and detection (*73*). Conventional anatomical images were collected using TurboFlash with slice-selective inversion (*74*). Typical imaging parameters were an inversion time ($T_1$) of 1.2 s, an echo time (TE) of 4.7 ms, and a repetition time of 9.6 ms. The field of view (FOV) was $22 \times 22$ cm$^2$ and the matrix size $256 \times 256$, which leads to an in-plane resolution of $0.86 \times 0.86$ mm$^2$; the slice thickness was 5 mm.

All functional imaging studies relied on $T_2^*$-weighted EPI (*75*) image acquisition (gradient echo; $64 \times 64$ matrix size, 30 ms for single-shot coverage of *k*-space, 3 s repetition time per multislice whole brain image set). fMRI data of usually 30 contiguous coronal slices (5 mm slice thickness, $22 \times 22$ cm$^2$ FOV) were acquired to cover the entire brain with a subsequent in-plane resolution of $3.4 \times 3.4$ mm$^2$. In all experiments, imaging data were acquired during three baseline and two task periods that were interleaved; 20 to 30 images at each coronal slice were acquired in each of the five consecutive periods. A total of 100–150 images were collected for each plane. In all studies, the multislice $T_1$-weighted TurboFlash images were acquired with the same FOV, slice positions, and orientations as in functional images for anatomical information. A motion detector was used to monitor the head motion (*76*). At the same time the heart cycle through a pulse oximeter (NONIN™) and respiration parameters were recorded on line.

BOLD fMRI data in *k*-space were Gaussian filtered, then Fourier transformed and analyzed using the functional imaging software, STIMULATE, developed in this laboratory.

BOLD maps for signal intensity changes were generated by comparison of $T_2^*$-weighted EPI images acquired between task and baseline periods using a period cross-correlation method (*77*). The correlation coefficient threshold used to create the functional maps was 0.2. Pixels with less than eight contiguous activated pixels were excluded from the functional maps; that is, an 8-pixel cluster was used.

The probability value $p$ for false positives showing activated pixels and taking into account multiple comparisons was calculated based on the method described by Xiong *et al.* (*78*). This method accounts for (i) the cluster size threshold; (ii) the intensity threshold of statistical significance (the $t$ value) used to define the activated pixels; (iii) the smoothness due to the Gaussian filtering; and (iv) the total number of pixels in the searched brain area used in the statistical analysis. It provides a more rigorous approach to evaluating activated areas in fMRI maps in comparison with Bonferroni-type corrections or conventional intensity-only thresholding methods. The smoothness factor, $|L|$, is a critical parameter used in these calculations and can be estimated experimentally or theoretically (*79*). Since previous work demonstrated that the first method gave an average $|L|$ value of 0.46 that differed by only 2% with the theoretical value, the theoretical $|L|$ value was used (*79*). Based on these parameters the effective $p$ value corresponding to a correlation coefficient of 0.2 was 0.007.

The individual maps were then normalized and warped to Talairach space (*80*). All anatomical assignments made in this study (listed on Table 1) are based on coordinates in Talairach space. An activation was considered bilateral if significant activation occurred in at least one slice bilaterally. To assess the pattern of activation occurring across a group of subjects, all individual functional maps were superimposed based on a pixel by pixel comparison. Pixels common to a predetermined minimum number of the subjects (e.g., four, five, or six out of six) were color coded to reflect the number of subjects which displayed activation in that pixel. The common pixels were displayed in a final composite functional map. This procedure is distinctly different from other approaches commonly used in PET studies, where raw image-space data are normalized and averaged to generate a single intersubject data set which is then analyzed for functional activation. It is also different from approaches where individual fMRI functional maps are added (*81*).

## ACKNOWLEDGMENTS

This work was supported in part by NIH Grants RRO8079 and NS31530, and the Human Frontier Science Program.

## REFERENCES

1. G. Schneider, Two visual systems: Brain mechanisms for localization and discrimination are dissociated by tectal and cortical lesions, *Science* **163,** 94–112 (1969).
2. L. G. Ungerleider and M. Mishkin, Two cortical visual systems, *in* ''Analysis of Visual Behavior'' (D. J. Ingle, M. A. Goodale, and R. J. W. Mansfield, Eds.), pp. 540–586, MIT Press, Cambridge, MA (1982).
3. S. M. Kosslyn, M. A. Alpert, W. L. Thompson, C. F. Chabris, S. L. Rauch, and A. K. Anderson, Identifying objects seen from different viewpoints. A PET investigation, *Brain* **117,** 1055–1071 (1994).
4. J. V. Haxby, B. Horwitz, L. G. Ungerleider, J. M. Maisong, P. Pietrini, and C. L. Grady, The functional organization of human extrastriate cortex: A PET-rCBF study of selective attention to faces and locations, *J. Neurosci.* **14,** 6336–6353 (1994).
5. S. Köhler, S. Kapur, M. Moscovitch, G. Winocur, and S. Houle, Dissociation of pathways for object and spatial vision: A PET study in humans, *NeuroReport* **6,** 1865–1868 (1995).
6. A. D. Milner and M. A. Goodale, Visual pathways to perception and action, *Prog. Brain Res.* **95,** 317–337 (1993).
7. A. D. Milner and M. Goodale, ''The Visual Brain in Action,'' Oxford Univ. Press, Oxford (1995).
8. S. P. Wise, D. Boussaoud, P. B. Johnson, and R. Caminiti, Primate premotor cortex: Corticocortical connectivity and combinatorial computations, *Ann. Rev. Neurosci.* **20,** 25–42 (1997).
9. J. V. Haxby, C. L. Grady, B. Horwitz, L. G. Ungerleider, M. Mishkin, R. E. Carson, P. Herscovitch, M. B. Schapiro, and S. I. Rapoport, Dissociation of object and spatial visual processing pathways in human extrastriate cortex, *Proc. Natl. Acad. Sci. USA* **88,** 1621–1625 (1991).
10. M. Corbetta, F. M. Miezin, G. L. Shulman, and S. E. Petersen, A PET study of visuospatial attention, *J. Neurosci.* **13,** 1202–1226 (1993).
11. S. Zeki, J. Watson, C. Lueck, K. Friston, C. Kennard, and R. Frackowiak, A direct demonstration of functional specialization in human visual cortex, *J. Neurosci.* **11,** 641–649 (1991).
12. S. Shipp, B. de Jong, J. Zihl, R. Frackowiak, and S. Zeki, The brain activity related to residual motion vision in a patient with bilateral lesions of V5, *Brain* **117,** 1023–1038 (1994).
13. E. Bonda, M. Petrides, D. Ostry, and A. Evans, Specific involvement of human parietal systems and the amygdala in the perception of biological motion, *J. Neurosci.* **16,** 3737–3744 (1996).
14. M. Sereno, A. Dale, J. Reppas, K. Kwong, J. Belliveau, T. Brady, B. Rosen, and R. Tootell, Borders of multiple visual areas in humans revealed by functional magnetic resonance imaging, *Science* **268,** 803–804 (1995).
15. R. B. H. Tootell, J. B. Reppas, A. M. Dale, R. B. Look, M. I. Sereno, R. Malach, T. J. Brady, and B. R. Rosen, Visual motion aftereffect in human cortical area MT revealed by functional magnetic resonance imaging, *Nature* **375,** 139–141 (1995).
16. R. B. Tootell, J. B. Reppas, K. K. Kwong, R. Malach, R. T. Born, T. J. Brady, B. R. Rosen, and J. W. Belliveau, Functional analysis of human MT and related visual cortical areas using magnetic resonance imaging, *J. Neurosci.* **15,** 3215–3230 (1995).
17. R. M. O'Craven, B. R. Rosen, K. K. Kwong, A. Treisman, and R. L. Savoy, Voluntary attention modulates fMRI activity in human MT-MST, *Neuron* **18,** 591–598 (1997).
18. P. Dupont, G. Orban, B. De Bruyn, A. Verbruggen, and L. Mortelmans, Many areas in the brain respond to visual motion, *J. Neurophysiol.* **72,** 1420–1424 (1994).
19. C. Kertzman, U. Schwarz, T. Zeffiro, and M. Hallett, The role of posterior parietal cortex in visually guided reaching movements in humans, *Exp. Brain Res.* **114,** 170–183 (1997).
20. D. Clower, J. Hoffmann, J. Votaw, T. Faber, R. Woods, and G. Alexander, Role of posterior parietal cortex in the recalibration of visually guided reaching, *Nature* **383,** 618–621 (1996).

21. M. P. Deiber, R. E. Passingham, J. G. Colebatch, K. J. Friston, P. D. Nixon, and R. S. J. Frackowiak, Cortical areas and the selection of movement: a study with positron emission tomography, *Exp. Brain Res.* **84,** 393–402 (1991).

22. S. T. Grafton, J. C. Mazziotta, R. P. Woods, and M. E. Phelps, Human functional anatomy of visually guided finger movements, *Brain* **115,** 565–587 (1992).

23. D. Flament, J. M. Ellermann, S.-G. Kim, K. Ugurbil, and T. J. Ebner, Functional magnetic resonance imaging of cerebellar activation during learning of a visuomotor dissociation task, *Human Brain Mapping* **4,** 210–226 (1996).

24. M. Glickstein, J. L. Cohen, B. Dixon, A. Gibson, M. Hollins, E. LaBossiere, and F. Robinson, Corticopontine visual projections in macaque monkeys, *J. Comp. Neurol.* **190,** 209–229 (1980).

25. J. Stein and M. Glickstein, Role of the cerebellum in visual guidance of movement, *Physiol. Rev.* **72,** 967–1017 (1992).

26. T. J. Ebner and Q.-G. Fu, What features of visually guided arm movements are encoded in the simple spike discharge of cerebellar Purkinje cells? *Prog. Brain Res.* **114,** 431–447 (1997).

27. J. G. May, Different patterns of corticopontine projections from separate cortical fields within the inferior parietal lobule and dorsal prelunate gyrus of macaque, *Exp. Brain Res.* **63,** 265–278 (1986).

28. M. Glickstein, J. May, and B. Mercier, Corticopontine projection in the macaque: The distribution of labelled cortical cells after large injections of horseradish peroxidase in the pontine nuclei, *J. Comp. Neurol.* **235,** 343–715 (1985).

29. S. Nakagawa and S. Tanaka, Retinal projections to the pulvinar nucleus of the macaque monkey: A re-investigation using autoradiography, *Exp. Brain Res.* **57,** 151–157 (1984).

30. D. L. Robinson and J. W. McClurkin, The visual superior colliculus and pulvinar, *in* ''The Neurobiology of Saccadic Eye Movement'' (R. H. Wurtz and M. E. Goldberg, Eds.), pp. 337–360, Elsevier, Amsterdam (1989).

31. C. Cavada and P. S. Goldman-Rakic, Multiple visual areas in the posterior cortex of primates, *in* ''Progress in Brain Research'' (T. P. Hicks, S. Molotchnikoff, and T. Ono, Eds.), pp. 123–137, Elsevier, Amsterdam (1993).

32. S. Ogawa and T. M. Lee, Magnetic resonance imaging of blood vessels at high fields: *In vivo* and *in vitro* measurements and image simulation, *Magn. Reson. Med.* **16,** 9–18 (1990).

33. K. K. Kwong, J. W. Belliveau, D. A. Chesler, I. E. Goldberg, R. M. Weisskoff, B. P. Poncelet, D. N. Kennedy, B. E. Hoppel, M. S. Cohen, R. Turner, H.-M. Cheng, T. J. Brady, and B. R. Rosen, Dynamic magnetic resonance imaging of human brain activity during primary sensory stimulation, *Proc. Natl. Acad. Sci. USA* **89,** 5675–5679 (1992).

34. S. Ogawa, D. W. Tank, R. Menon, J. M. Ellermann, S.-G. Kim, H. Merkle, and K. Ugurbil, Intrinsic signal changes accompanying sensory stimulation: Functional brain mapping with magnetic resonance imaging, *Proc. Natl. Acad. Sci. USA* **89,** 5951–5955 (1992).

35. P. A. Bandettini, E. C. Wong, R. S. Hinks, R. S. Tikofsky, and J. S. Hyde, Time course EPI of human brain function during task activation, *Magn. Reson. Med.* **25,** 390–398 (1992).

36. A. M. Blamire, S. Ogawa, K. Ugurbil, D. Rothman, G. McCarthy, J. M. Ellermann, F. Hyder, Z. Rattner, and R. G. Shulman, Dynamic mapping of the human visual cortex by high-speed magnetic resonance imaging, *Proc. Natl. Acad. Sci. USA* **89,** 11,069–11,073 (1992).

37. J. Frahm, H. Bruhn, and K. D. Merboldt, Dynamic MRI of human brain oxygenation during rest and photic stimulation, *J. Magn. Reson. Imaging* **2,** 501–505 (1992).

38. P. T. Fox and M. E. Raichle, Focal physiological uncoupling of cerebral blood flow and oxidative metabolism during somatosensory stimulation in human subjects, *Proc. Natl. Acad. Sci. USA* **83,** 1140–1144 (1986).

39. P. T. Fox, M. E. Raichle, M. A. Mintun, and C. Dence, Nonoxidative glucose consumption during focal physiologic neural activity, *Science* **241,** 462–464 (1988).

40. N. F. Ramsey, B. Kirby, P. Van Gelderen, K. Berman, C. T. W. Monen, V. S. Mattay, J. A. Fran, J. Van Horn, G. Esposito, and D. R. Weinberger, A direct comparison of 3D BOLD fMRI and $H_2{}^{15}O$ PET imaging of primary sensory motor cortex in humans, *in* ''3rd Scientific Meeting of the Society of Magnetic Resonance in Medicine,'' Vol. 2, p. 1324 (1995).

41. A. Connelly, C. Dettmers, K. M. Stephan, R. Turner, K. J. Friston, R. S. J. Frackowiak, and D. G. Gadian, Quantitative comparison of functional magnetic resonance imaging and positron emission tomography using a controlled-force motor paradigm, *in* ''3rd Scientific Meeting of the International Society of Magnetic Resonance in Medicine, Vol. 2, p. 786 (1995).

42. S.-G. Kim, Quantification of relative cerebral blood flow change by flow-sensitive alternating inversion recovery (FAIR) technique: Application to functional mapping, *Magn. Reson. Med.* **34,** 293–301 (1995).

43. J. D. Siegal, J. M. Ellermann, P. Erhard, J. P. Strupp, K. Ugurbil, and T. J. Ebner, Functional MRI (fMRI) activation of cortical and cerebellar pathways during the performance of visually guided motor tasks, *NeuroImage* **3,** S415 (1996).

44. J. Ellermann, J. Siegal, T. Ebner, and K. Ugurbil, Functional MRI evidence of dorsal stream activation in the human brain during the performance of a visually guided motor task, *in* ''5th Scientific Meeting of the International Society of Magnetic Resonance in Medicine,'' Vol. 1, p. 9 (1997).

45. J. Watson, R. Myers, R. Frackowiak, J. Hajnal, R. Woods, J. Mazziotta, S. Shipp, and S. Zeki, Area V5 of the human brain: Evidence from a combined study using positron emission tomography and magnetic resonance imaging, *Cerebral Cortex* **3,** 79–94 (1993).

46. C. Distler, D. Boussaoud, R. Desimone, and L. G. Ungerleider, Cortical connections of inferior temporal and TEO in macaque monkeys, *J. Comp. Neurol.* **334,** 125–150 (1993).

47. D. Boussaoud, L. G. Ungerleider, and R. Desimone, Pathways for motion analysis: Cortical connections of the medial superior temporal and fundus of the superior temporal visual areas of the macaque, *J. Comp. Neurol.* **296,** 462–495 (1990).

48. M. Taira, S. Mine, A. P. Georgopoulos, A. Murata, and H. Sakata, Parietal cortex neurons of the monkey related to the visual guidance of hand movement, *Exp. Brain Res.* **83,** 29–36 (1990).

49. C. L. Colby and J.-R. Duhamel, Heterogeneity of extrastriate visual areas and multiple parietal areas in the macaque monkey, *Neuropsychologia* **29,** 517–537 (1991).

50. R. Caminiti, S. Ferraina, and P. B. Johnson, The sources of visual information to the primate frontal lobe: A novel role for the superior parietal lobule, *Cerebral Cortex* **6,** 319–328 (1996).

51. R. Andersen, G. Essick, and R. Siegel, Encoding of spatial location by posterior parietal neurons, *Science* **230,** 456–458 (1985).

52. P. Brotchie, R. Andersen, L. Snyder, and S. Goodman, Head position signals used by parietal neurons to encode locations of visual stimuli, *Nature* **375,** 232–235 (1995).

53. J. Sweeney, M. Mintun, S. Kwee, M. Wiseman, D. Brown, D. Rosenberg, and J. Carl, Positron emission tomography study of voluntary saccadic eye movements and spatial working memory, *J. Neurophysiol.* **75,** 454–468 (1996).

*54.* J. H. R. Maunsell and D. C. Van Essen, Functional properties of neurons in middle temporal visual area of macaque monkey. I. Selectivity for stimulus direction, speed and orientation, *J. Neurophysiol.* **49,** 1127–1147 (1983).

*55.* H. Sakata and M. Taira, Parietal control of hand action, *Curr. Opin. Neurobiol.* **4,** 847–586 (1994).

*56.* J. Jonides, E. Smith, R. Koeppe, E. Awh, S. Minoshima, and M. Mintun, Spatial working memory in humans as revealed by PET, *Nature* **363,** 583–584 (1993).

*57.* M. Corbetta, G. Shulman, F. Miezin, and S. Petersen, Superior parietal cortex activation during spatial attention shifts and visual feature conjunction, *Science* **270,** 802–805 (1995).

*58.* M. Posner, J. Walker, F. Friedrich, and R. Rafael, Effects of parietal lobe injury on covert orienting of attention, *J. Neurosci.* **4,** 1863–1874 (1984).

*59.* P. Brodal, The cerebro-ponto-cerebellar pathway: Salient features of its organization, *Exp. Brain Res. Suppl.* **6,** 108–133 (1982).

*60.* P. Brodal and J. Bjaalie, Quantitative studies of pontine projections from visual cortical areas in the cat, *in* ''Cerebellum and Neuronal Plasticity'' (M. A. S. Glickstein, Ed.), pp. 41–62, Plenum, New York (1987).

*61.* M. Glickstein, Brain pathways in visual guidance of movement, *in* ''Brain Circuits and Functions of the Mind'' (C. Trevarthen, Ed.), pp. 157–167, Cambridge Univ. Press, Cambridge, UK (1990).

*62.* J. S. Baizer, L. G. Ungerleider, and R. Desimone, Organization of visual inputs to the inferior temporal and posterior parietal cortex, *J. Neurosci.* **11,** 168–190 (1991).

*63.* C. Cavada and P. S. Goldman-Rakic, Topographic segregation of corticostriatal projections from posterior parietal subdivisions in the macaque monkey, *Neuroscience* **42,** 683–696 (1991).

*64.* R. Caminiti, P. B. Johnson, C. Galli, S. Ferraina, and Y. Burnod, Making arm movements within different parts of space: the premotor and motor cortical representation of a coordinate system for reaching to visual targets, *J. Neurosci.* **11,** 1182–1197 (1991).

*65.* D. Robinson and S. Petersen, The pulvinar and visual salience, *Trends Neurosci.* **15,** 127–132 (1992).

*66.* L. A. Benevento and G. P. Standage, The organization of projections of the retinorecipient and nonretinorecipient nuclei of the pretectal complex and layers of the superior colliculus to the lateral pulvinar and medial pulvinar in the macaque monkey, *J. Comp. Neurol.* **217,** 307–336 (1983).

*67.* C. G. Gross, Contribution of striate cortex and the superior colliculus to visual function in area MT, the superior temporal polysensory area and inferior temporal cortex, *Neuropsychologia* **29,** 497–515 (1991).

*68.* S. Petersen, D. Robinson, and W. Keys, Pulvinar nuclei of the behaving rhesus monkey: Visual responses and their modulation, *J. Neurophysiol.* **54,** 867–886 (1985).

*69.* S. Petersen, D. Robinson, and J. Morris, Contribution of the pulvinar to visual spatial attention, *Neuropsychologia* **25,** 97–105 (1987).

*70.* M. Bushnell, M. Goldberg, and D. Robinson, Behavioral enhancement of visual responses in monkey cerebral cortex. I. Modulation in posterior parietal cortex related to selective visual attention, *J. Neurophysiol.* **46,** 755–772 (1981).

*71.* A. Georgopoulos, J. Kalaska, R. Caminiti, and J. Massey, On the relations between the direction of two-dimensional arm movements and cell discharge in primate motor cortex, *J. Neurosci.* **2,** 1527–1537 (1982).

*72.* Q. Fu, J. Suarez, and T. Ebner, Neuronal specification of direction and distance during reaching movements in the superior precentral premotor area and primary motor cortex of monkeys, *J. Neurophysiol.* **70,** 2097–2116 (1993).

*73.* G. Adriany, J. T. Vaughan, P. Andersen, H. Merkle, M. Garwood, and K. Ugurbil, Comparison between head volume coils at high fields, *in* ''3rd Scientific Meeting of the International Society of Magnetic Resonance in Medicine,'' Vol. 2, p. 971 (1995).

*74.* A. Haase, Snapshot FLASH MRI: Application to T1-, T2-, and chemical shift imaging, *J. Magn. Reson.* **13,** 77–89 (1990).

*75.* P. Mansfield, Multi-planar image formation using NMR spin echoes, *J. Phys. C* **10,** L55–L58 (1977).

*76.* W. Chen, H. Merkle, P. Erhard, and K. Ugurbil, A robust device for monitoring head movement during functional MRI studies, *in* ''3rd Scientific Meeting of the International Society of Magnetic Resonance in Medicine,'' Vol. 3, p. 747 (1995).

*77.* P. A. Bandettini, A. Jesmanowicz, E. C. Wong, and J. S. Hyde, Processing strategies for time-course data sets in functional MRI of human brain, *Magn. Reson. Med.* **30,** 161–173 (1993).

*78.* J. Xiong, J. Gao, J. Lancaster, and P. Fox, Clustered pixels analysis for functional MRI activation studies of the human brain, *Human Brain Mapping* **3,** 287–301 (1995).

*79.* W. Chen, T. Kato, X. Zhu, P. Strupp, S. Ogawa, and K. Ugurbil, Mapping of lateral geniculate nucleus activation during visual stimulation in human brain using f MRI, *Magn. Reson. Med.* **39,** 89–96 (1998).

*80.* J. Talairach and P. Tournoux, ''Co-planar Stereotaxic Atlas of the Human Brain,'' Thieme Med Pub, New York (1988).

*81.* J. Binder, J. Frost, T. Hammeke, R. Cox, S. Rao, and T. Prieto, Human brain language areas identified by functional magnetic resonance imaging, *J. Neurosci.* **17,** 353–362 (1997).